OBTAINING THE COHESIVE LAWS OF A TRAPEZOIDAL MIXED-MODE DAMAGE MODEL USING AN INVERSE METHOD

RAUL D.S.G. CAMPILHO[1]*, MARCELO F.S.F. de MOURA[2]*, DIMITRA A. RAMANTANI[3]*, JOÃO P.M. GONÇALVES[4]**

*Universidade do Porto, Departamento de Engenharia Mecânica e Gestão Industrial, Faculdade de Engenharia, Rua Dr. Roberto Frias s/n, 4200-465 Porto, Portugal

**Mathematical Sciences Department, IBM T. J. Watson Research Center, 1101 Kitchawan Road, Yorktown Heights, NY 10598, USA

[1]dem05004@fe.up.pt, [2]mfmoura@fe.up.pt, [3]dem06002@fe.up.pt, [4]jpgoncal@us.ibm.com

ABSTRACT: The use of cohesive damage models in fracture problems has become frequent in recent years. The objective of this work is to present a trapezoidal mixed-mode cohesive damage model appropriate for ductile adhesives in adhesively bonded joints. The proposed model replaces the solid finite elements traditionally used to simulate the adhesive layer, thus reducing the computational effort. It is known that the adhesive bulk properties are not adequate to characterize these laws. In this work, Double Cantilever Beam and End Notched Flexure tests are performed to obtain the cohesive laws of the adhesive Araldite® 2015 in pure modes I and II, respectively. The fracture energies are obtained using a new data reduction scheme based on the crack equivalent concept. The remaining cohesive parameters are obtained with an inverse method. It was verified that the numerical *R*-curves agree with the experimental ones.

Keywords: Finite Element Method, Cohesive damage models, Bonded joints, Fracture.

RESUMO: A utilização de modelos de dano coesivos para a modelação de problemas de fractura tornou-se frequente nos últimos anos. O objectivo deste trabalho é apresentar um modelo de dano coesivo trapezoidal em modo misto adequado para adesivos dúcteis em juntas adesivas. O modelo proposto substitui os elementos finitos sólidos usados tradicionalmente para simular a camada de adesivo, reduzindo assim o esforço computacional. As propriedades medidas em provetes de adesivo maciço não são representativas do comportamento do adesivo quando utilizado na forma de camada muito fina. Assim, para caracterizar as leis coesivas do adesivo Araldite® 2015 em modos puros I e II realizaram-se ensaios Double Cantilever Beam e End Notched Flexure, respectivamente. As tenacidades são obtidas através de um método baseado no conceito da fenda equivalente. Os restantes parâmetros coesivos são obtidos por um método inverso. Verificou-se que as curvas *R* numéricas apresentam uma boa correlação com as experimentais.

Palavras chave: Método dos Elementos Finitos, Modelos de dano coesivos, Juntas coladas, Fractura.

1. INTRODUCTION

Adhesively bonded joints are being increasingly used in the last decades due to their interesting characteristics. Adhesive joints present a high fatigue strength, do not alter significantly the structure shape and present less stress concentrations than alternative techniques. Therefore, it is essential to predict accurately the joints' strength. The stress based methods are not adequate to predict the joint strength when stress singularities are present nor allow obtaining the failure paths. The fracture mechanics approach is frequently applied by means of an energetic analysis, overcoming these limitations. In this context, the determination of the critical fracture energies (J_{ic}, i=I, II) and the respective cohesive laws is essential.

Several authors studied the fracture behaviour of bonded joints in mode I. Blackman et al. [1] used a cohesive zone model (CZM) approach on Tapered Double Cantilever Beam (TDCB) and peel tests under mode I load including two parameters, G_c and σ_{max}, to study the fracture of adhesively bonded joints. A polynomial traction-separation law was considered. The main objective was to investigate the physical significance of σ_{max}. It was concluded that the specimen compliance and G_c depend on σ_{max} until a relatively high value of this parameter, when this dependence significantly diminished. Andersson and Stigh [2] used an inverse method to determine the cohesive parameters of a ductile adhesive layer loaded in peel using a Double Cantilever Beam (DCB) specimen. It was concluded that the respective stress-relative displacement curve can be divided in three parts. Initially a linear elastic behaviour is

observed. A plateau region is then observed, corresponding to the plastic behaviour. The curve ends with a parabolic softening part. In mode II, the End Notched Flexure (ENF) test is widely used. de Moura [3] performed a two-dimensional numerical study including a cohesive damage model on the ENF test, for mode-II fracture characterization of adhesive joints. The author concluded that the data reduction schemes based on beam theories, i.e., the Direct Beam Theory (DBT) and Corrected Beam Theory (CBT), produce some non-negligible errors. A new data reduction scheme was proposed, including the Fracture Process Zone (FPZ) effects and not depending on the crack length measurement. Leffler et al. [4] determined the complete stress versus deformation relation of a thin adhesive layer loaded in shear, using the ENF specimen. The method included the determination of the energy release rate as a function of the shear deformation at the crack tip, followed by derivation of the traction-separation relation using an inverse method. An approximate trapezoidal relation was obtained.

Fracture characterization in pure mode I and II is usually performed using the DCB specimen [1, 5, 6] and the ENF specimen [3], respectively. The main advantages of these experimental tests are their simplicity and the possibility to obtain J_{ic} mathematically using the beam theory [3, 7]. However, some issues must be taken into account to measure accurately J_{Ic}, especially when ductile adhesives are used. In fact, in the DCB test, the crack tip may not be clearly visible depending on the adhesive. This can induce non negligible errors on the derivative of the compliance relatively to the crack length (dC/da) used in the Compliance Calibration Method (CCM). On the other hand, the energy dissipated at the FPZ is significant, especially when using ductile adhesives. In mode II tests, one of the most significant difficulties is the crack length monitoring, since propagation occurs rapidly and without a clear opening. Moreover, identification of the crack tip can be ambiguous, owing to microcracks in the relatively large FPZ [8].

The objective of this work is to obtain trapezoidal cohesive laws in pure modes I and II for a ductile adhesive layer to be applied in numerical simulations of bonded joints. These laws are implemented within interface finite elements, replacing the solid finite elements traditionally used to simulate the adhesive layer, thus reducing the computational effort. It is known that the adhesive bulk properties are not adequate to characterize these laws. In this work, DCB and ENF tests are used to obtain the cohesive laws of the adhesive Araldite® 2015 in pure modes I and II, respectively. J_{ic} (i=I, II) are obtained using a new data reduction scheme based on the crack equivalent concept. The method only requires an accurate measurement of the compliance during the test and is named Compliance-Based Beam Theory (CBBM). An excellent agreement was found between the experimental and numerical R-curves. The remaining cohesive parameters are obtained with an inverse method, fitting the numerical P-δ curves with the experiments and allowing complete fracture characterization of the adhesive Araldite® 2015 in pure modes I and II.

2. EXPERIMENTAL WORK

The geometry and dimensions of the DCB and ENF specimens is presented in Fig. 1 a) and b), respectively. Unidirectional 0º lay-ups of carbon/epoxy prepreg (SEAL™ Texipreg HS 160 RM) adherends with 0.15 mm ply thickness were used, whose mechanical properties are presented in Table 1 [9]. Curing was achieved in a press during one hour at 130ºC and 4 bar pressure. The ductile epoxy adhesive Araldite® 2015 was used, whose elastic properties were measured experimentally in bulk tests (E=1850 MPa, ν=0.3). The bonded surfaces were abraded with sandpaper, and cleaned with acetone to avoid adhesive failures [9], followed by assembly and holding with contact pressure and curing at room temperature. Five specimens of each geometry were tested, using an INSTRON testing machine at room temperature under displacement control (2 mm/min). The load-displacement (P-δ) curve was registered during the test. Pictures were recorded during the specimens testing with 5 s intervals using a 10 MPixel digital camera. This procedure allows measuring the crack length during its growth and afterwards collecting the P-δ-a parameters. This was performed correlating the time elapsed since the beginning of each test between the P-δ curve and each picture (the testing time of each P-δ curve point is obtained accurately with the absolute displacement and the established loading rate).

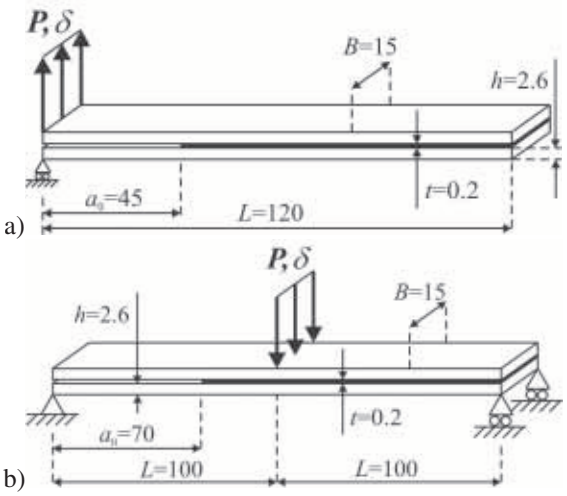

Fig. 1. Geometry of the DCB (a) and ENF (b) specimens (dimensions in mm).

Table 1. Carbon-epoxy ply elastic properties.

E_1=1.09E+05 MPa	ν_{12}=0.342	G_{12}=4315 MPa
E_2=8819 MPa	ν_{13}=0.342	G_{13}=4315 MPa
E_3=8819 MPa	ν_{23}=0.380	G_{23}=3200 MPa

3. COMPLIANCE BASED BEAM METHOD

The DCB and the ENF specimens were used to obtain J_{Ic} and J_{IIc}, respectively. The classical methods depend on accurate crack length measurements during propagation. However, a FPZ develops ahead of the crack tip in consequence of the nucleation of multiple micro-cracks

through the adhesive thickness and plastification. This phenomenon renders difficult to locate the crack tip accurately. Moreover, the energy dissipated in the FPZ should be taken into account in the selected data reduction scheme. To overcome these difficulties a new data reduction scheme based on the crack equivalent concept, and depending only on the specimen's compliance, is presented for the two fracture characterization tests.

DCB specimen

From the Castigliano theorem, the displacement δ can be written as follows, using the strain energy of the DCB specimen (Fig. 1 a)

$$\delta = \frac{\partial U}{\partial P} = \frac{8Pa^3}{E_1 Bh^3} + \frac{12Pa}{5BhG_{13}} \tag{1}$$

This equation constitutes an approach based on beam theory and allows defining the compliance $C=\delta/P$ of the specimen. However, some issues like stress concentrations at the crack tip, influencing the P-δ curve, are not accounted for in the beam theory. To overcome these discrepancies, a corrected flexural modulus can be used instead of E_1. The flexural modulus of the specimen can be obtained from equation (1) using the measured initial compliance (C_0)

$$E_f = \left(C_0 - \frac{12\left(a_0 + |\Delta|\right)}{5BhG_{13}} \right)^{-1} \frac{8\left(a_0 + |\Delta|\right)^3}{Bh^3} \tag{2}$$

where Δ is the root rotation correction for the initial crack length, obtained from the linear regression of $C^{1/3}=f(a_0)$. On the other hand, an equivalent crack length (a_{eq}) must be considered during propagation to account for the FPZ effects at the crack tip. The equivalent crack can be calculated from equation (1) as a function of the specimen's compliance registered during the test and considering $a_{eq} = a + |\Delta| + \Delta a_{FPZ}$ instead of a. J_{Ic} can now be obtained using the Irwin-Kies equation, which leads to

$$J_{Ic} = \frac{6P^2}{B^2 h}\left(\frac{2a_{eq}^2}{h^2 E_f} + \frac{1}{5G_{13}} \right) \tag{3}$$

ENF specimen

Following a similar procedure for mode II using the ENF specimen (Fig. 1 b), the compliance equation can be written as

$$C = \frac{3a^3 + 2L^3}{12E_1 I} + \frac{3L}{10G_{13}Bh} \tag{4}$$

The flexural modulus in this case can be obtained using the initial compliance C_0 and the initial crack length a_0

$$E_f = \frac{3a_0^3 + 2L^3}{12I}\left(C_0 - \frac{3L}{10G_{13}Bh} \right)^{-1} \tag{5}$$

The effect of the FPZ can be included considering the compliance and the equivalent crack concept during propagation. Combining equations (4) and (5) it can be written

$$a_{eq} = a + \Delta a_{FPZ} = \left[\frac{C_{corr}}{C_{0corr}} a_0^3 + \frac{2}{3}\left(\frac{C_{corr}}{C_{0corr}} - 1 \right) L^3 \right]^{1/3} \tag{6}$$

where C_{corr} is given by

$$C_{corr} = C - \frac{3L}{10G_{13}Bh} \tag{7}$$

J_{IIc} can now be obtained using the Irwin-Kies equation

$$J_{IIc} = \frac{9P^2 a_{eq}^2}{16B^2 E_f h^3} \tag{8}$$

The presented methodology allows obtaining J_{ic} (i=I, II) using only the P-δ curve. For this reason it is named Compliance-Based Beam Method. Using this method it is not necessary to measure the crack length during propagation because the calculated equivalent crack length is used instead of the real one. Another advantage is related to the fact that a_{eq} includes the effect of the FPZ, not taken into account when the real crack length is considered.

4. TRAPEZOIDAL COHESIVE DAMAGE MODEL

A cohesive mixed-mode (I+II) damage model based on interface finite elements was developed to simulate damage onset and growth. The adhesive is simulated by these elements, which have zero thickness. To simulate the behaviour of ductile adhesives, a trapezoidal softening law between stresses (σ) and relative displacements (δ_r) between homologous points of the interface elements was employed (Fig. 2).

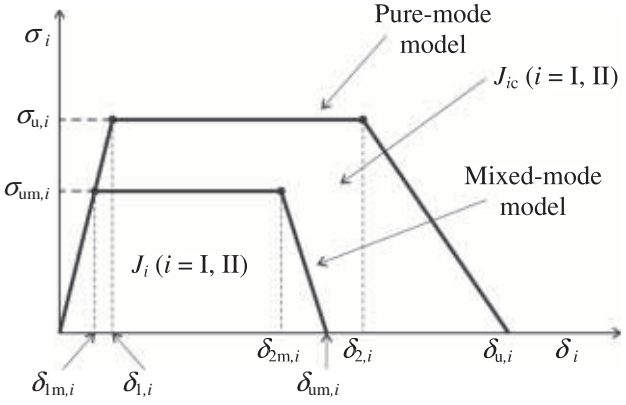

Fig. 2. The trapezoidal softening law for pure-mode and mixed-mode.

The constitutive relationship before damage onset is

$$\boldsymbol{\sigma} = \mathbf{E}\boldsymbol{\delta}_r \tag{9}$$

where **E** is a stiffness diagonal matrix containing the stiffness parameters e_i (i=I, II) defined as the ratio between the elastic modulus of the material in tension or shear (E or G, respectively) and the adhesive thickness t. Considering the pure-mode model, after $\delta_{1,i}$ (the first inflexion point, which leads to the plateau region of the trapezoidal law) the material softens progressively. The softening relationship can be written as

$$\boldsymbol{\sigma} = (\mathbf{I} - \mathbf{D})\mathbf{E}\boldsymbol{\delta}_{\mathbf{r}} \tag{10}$$

where **I** is the identity matrix and **D** is a diagonal matrix containing, on the position corresponding to mode i (i=I, II) the damage parameter. In general, bonded joints or repairs are subjected to mixed-mode loading. Therefore, a formulation for interface finite elements should include a mixed-mode damage model (Fig. 2). Damage onset is predicted using a quadratic stress criterion

$$\begin{aligned} &\left(\frac{\sigma_{\mathrm{I}}}{\sigma_{\mathrm{u,I}}}\right)^2 + \left(\frac{\sigma_{\mathrm{II}}}{\sigma_{\mathrm{u,II}}}\right)^2 = 1 \quad \text{if} \quad \sigma_{\mathrm{I}} > 0 \\ &\sigma_{\mathrm{II}} = \sigma_{\mathrm{u,II}} \qquad\qquad\quad \text{if} \quad \sigma_{\mathrm{I}} \le 0 \end{aligned} \tag{11}$$

where σ_i, (i=I, II) represent the stresses in each mode. It is assumed that normal compressive stresses do not induce damage. Considering equation (9), the first equation (11) can be rewritten as a function of the relative displacements

$$\left(\frac{\delta_{\mathrm{1m,I}}}{\delta_{\mathrm{1,I}}}\right)^2 + \left(\frac{\delta_{\mathrm{1m,II}}}{\delta_{\mathrm{1,II}}}\right)^2 = 1 \tag{12}$$

where $\delta_{1\mathrm{m},i}$ (i=I, II) are the relative displacements in each mode corresponding to damage initiation. Stress softening onset ($\delta_{2,i}$) was predicted using a quadratic relative displacements criterion similar to (12), leading to

$$\left(\frac{\delta_{\mathrm{2m,I}}}{\delta_{\mathrm{2,I}}}\right)^2 + \left(\frac{\delta_{\mathrm{2m,II}}}{\delta_{\mathrm{2,II}}}\right)^2 = 1 \tag{13}$$

where $\delta_{2\mathrm{m},i}$ (i=I, II) are the relative displacements in each mode corresponding to stress softening onset. Crack growth was simulated by the linear fracture energetic criterion

$$\frac{J_{\mathrm{I}}}{J_{\mathrm{Ic}}} + \frac{J_{\mathrm{II}}}{J_{\mathrm{IIc}}} = 1 \tag{14}$$

When equation (14) is satisfied damage growth occurs and stresses are completely released, with the exception of normal compressive ones. Using the proposed criteria (equations (12), (13) and (14)), it is possible to define $\delta_{1\mathrm{m}}$, $\delta_{2\mathrm{m}}$ and δ_{um} and establishing the damage parameters in the plateau region

$$d_{\mathrm{m}} = 1 - \frac{\delta_{\mathrm{1,m}}}{\delta_{\mathrm{m}}} \tag{15}$$

and in the stress softening part of the cohesive law

$$d_{\mathrm{m}} = 1 - \frac{\delta_{\mathrm{1,m}}\left(\delta_{\mathrm{u,m}} - \delta_{\mathrm{m}}\right)}{\delta_{\mathrm{m}}\left(\delta_{\mathrm{u,m}} - \delta_{\mathrm{2,m}}\right)} \tag{16}$$

A detailed description of the model is presented in the work of Campilho et al. [10].

5. EXPERIMENTAL RESULTS

J_{ic} were obtained experimentally using the CBBM and the CBT (Table 2). For the DCB specimens, similar results were obtained using both methods. The results obtained for the ENF specimens also reveal a good agreement.

Table 2. J_{ic} obtained by the DCB and ENF tests.

	J_{Ic} (DCB tests)		J_{IIc} (ENF tests)	
Specimen	CBT	CBBM	CBT	CBBM
1	0.45	0.44	4.85	4.94
2	0.42	0.42	4.86	5.13
3	0.44	0.40	4.48	4.82
4	0.40	0.41	4.31	4.28
5	0.45	0.47	4.31	4.40
Avg. J_{ic}	0.43	0.43	4.56	4.71
St. Dev.	0.02	0.02	0.25	0.32

6. DETERMINATION OF THE TRAPEZOIDAL LAWS

The determination of J_{ic} (i=I, II) was performed experimentally using the CBBM. The remaining cohesive parameters were obtained by an inverse method. This method consisted on inputting each J_{ic} in the respective DCB or ENF numerical model including the trapezoidal mixed-mode cohesive damage model simulating the adhesive layer. In the following step, a fitting iterative procedure of the numerical and experimental P-δ curves allows defining the remaining cohesive parameters ($\sigma_{\mathrm{u},i}$ and $\delta_{2,i}$). Fig. 3 and Fig. 4 show the trapezoidal cohesive laws range in pure modes I and II, respectively, and the average values of J_{ic}, $\delta_{2,i}$ and $\delta_{\mathrm{u},i}$ (i=I, II).

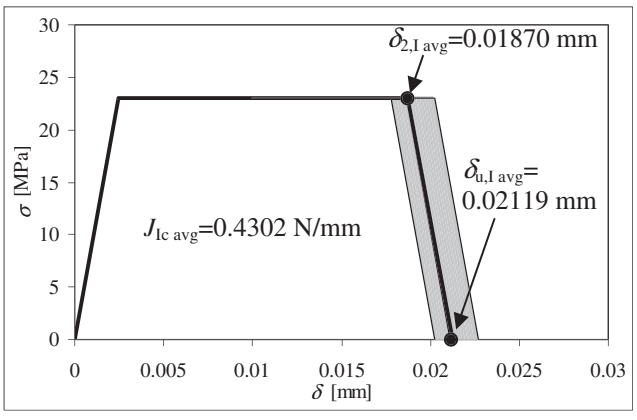

Fig. 3. Trapezoidal cohesive laws range in pure mode I of the DCB tests.

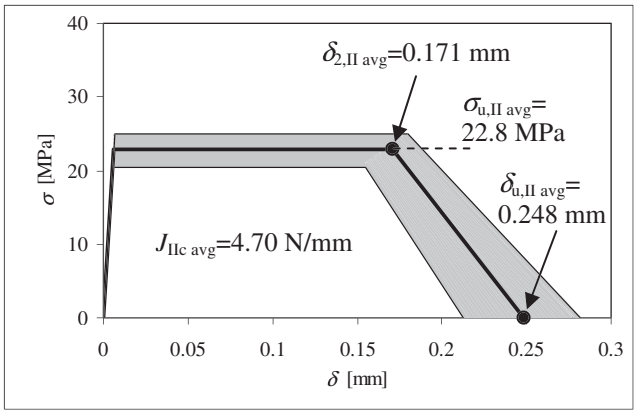

Fig. 4. Trapezoidal cohesive laws range in pure mode II of the ENF tests.

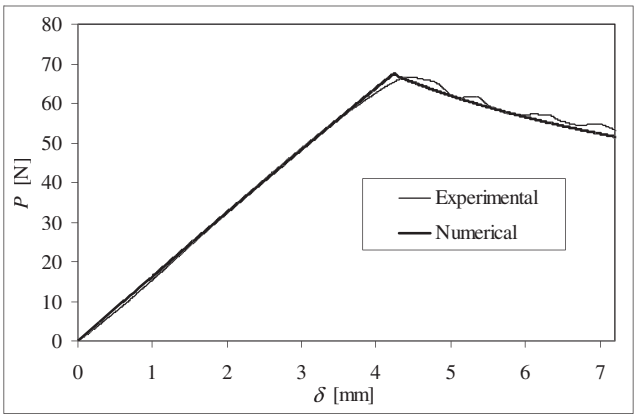

Fig. 5. Numerical and experimental P-δ curves for one DCB specimen.

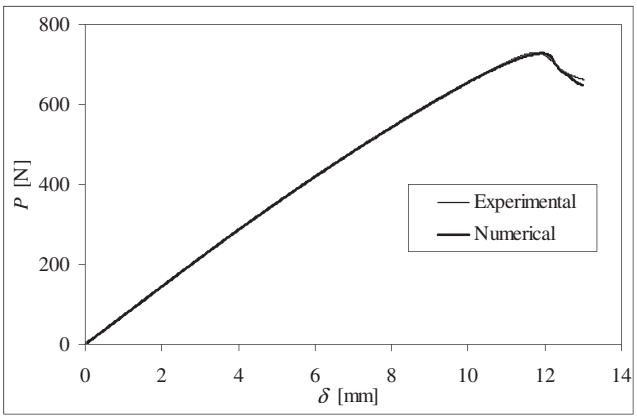

Fig. 6. Numerical and experimental P-δ curves for one ENF specimen.

The cohesive laws were inputted in the numerical models to simulate the adhesive layer. Fig. 5 and Fig. 6 present for one DCB and ENF specimen, respectively, a comparison between the experimental P-δ curves, and the numerical ones including the respective cohesive laws. Fig. 7 and Fig. 8 show a comparison between the numerical and experimental R-curves for one tested DCB and ENF specimen, respectively, using the CBBM. The excellent agreement in both cases proves this method adequacy in order to measure J_{ic}.

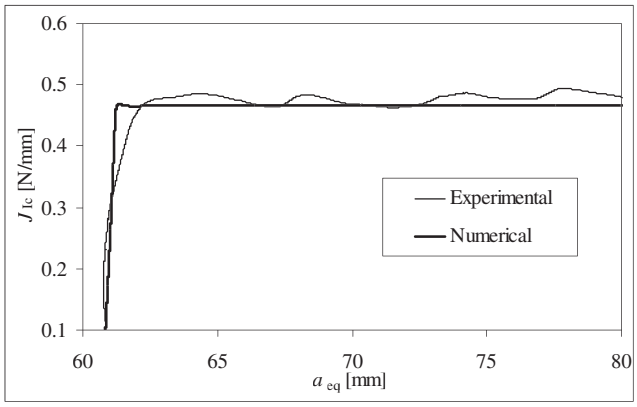

Fig. 7. Numerical and experimental R-curves on one DCB specimen.

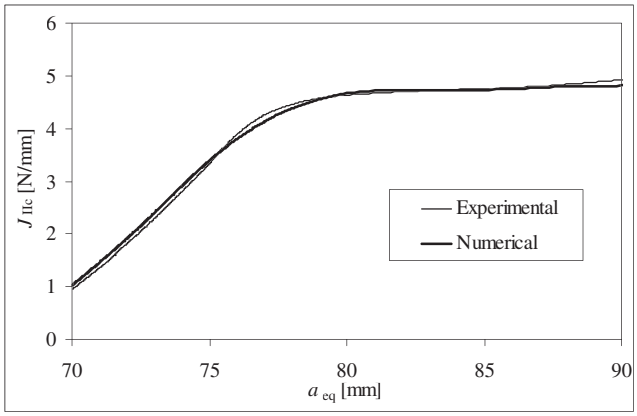

Fig. 8. Numerical and experimental R-curves on one ENF specimen.

Table 3. Inputted and predicted J_{Ic} values using DCB numerical models.

Specimen	Inputted	CBT	Error [%]	CBBM	Error [%]
1	0.444	0.448	1.0	0.442	-0.5
2	0.420	0.422	0.5	0.416	-0.9
3	0.415	0.423	2.0	0.413	-0.5
4	0.406	0.410	0.9	0.405	-0.3
5	0.468	0.472	0.8	0.466	-0.3
Avg. Error [%]		1.0		0.5	

Table 4. Inputted and predicted J_{IIc} values using ENF numerical models.

Specimen	Inputted	CBT	Error [%]	CBBM	Error [%]
1	4.94	3.51	-28.9	4.89	-0.9
2	5.13	3.62	-29.3	5.07	-1.2
3	4.82	3.42	-29.1	4.80	-0.5
4	4.28	3.06	-28.5	4.26	-0.4
5	4.32	3.03	-29.9	4.31	-0.2
Avg. Error [%]		29.15		0.60	

Numerical simulations of the DCB and ENF tests were performed to verify how the used methods replicate the inputted J_{ic}. The numerical P-δ-a parameters were collected to obtain the respective R-curves. Table 3 and Table 4 show the results for the DCB and ENF specimens, respectively. The average error corresponds to the average of the absolute individual error values. For the DCB test, excellent agreement was obtained between the predicted and inputted values. However, it should be noted that the CBT requires the crack length monitoring during propagation, which is not easy to perform experimentally and is prone to introduce additional errors. Moreover, the CBBM provides a complete R-curve and accounts for the energy dissipation at the FPZ. For the ENF test, the CBBM gives good results, while the CBT clearly underestimates the inputted J_{IIc} [3].

7. CONCLUDING REMARKS

In this work a suitable methodology of fracture characterization under pure modes I and II of ductile adhesives used in bonded joints is performed. A new data reduction scheme based on the crack equivalent concept is used to obtain the critical fracture energies with the DCB and ENF tests. The method is advantageous relatively to classical ones as it does not require the crack length measurement during its growth and accounts for the energy dissipated at the FPZ, which can be non negligible when ductile adhesives are used. A numerical analysis was also performed to verify the adequacy of different methods on the measurement of the critical fracture energies. A trapezoidal mixed-mode cohesive damage model was developed to simulate the behaviour of ductile adhesives. An inverse method was used to define the cohesive parameters of the trapezoidal laws. The comparison between the numerical and experimental results showed that the proposed CBBM provides accurate results on the critical fracture energies. Due to its advantages it can be considered the best choice for the fracture characterization of bonded joints.

.

ACKNOWLEDGEMENTS

The authors thank the Portuguese Foundation for Science and Technology for supporting the work here presented, through the Research Project POCI/EME/56567/2004 and the individual grant SFRH/BD/30305/2006.

REFERENCES

[1] B. R. K. Blackman, H. Hadavinia, A. J. Kinloch and J. G. Williams, *Int. J. Fract.* **119** (2003) 25.

[2] T. Andersson and U. Stigh, *Int. J. Sol. Struct.* **41** (2004) 413.

[3] M. F. S. F. de Moura, *J. Adh. Sci. Technol.* **20** (2006) 37.

[4] K. Leffler, K. S. Alfredsson and U. Stigh, *Int. J. Sol. Struct.* **44** (2007) 530.

[5] M. G. Bader, I. Hamerton, J. N. Hay, M. Kemp and S. Winchester, *Comp. Part A* **31** (2000) 603.

[6] J. Schön, T. Nyman, A. Blom and H. Ansell, *Comp. Sci. Technol.* **60** (2000) 173.

[7] H. Yoshihara, *Holzforschung* **61** (2007) 182.

[8] C. R. Corleto and W. L. Bradley, *ASTM STP* **341** (1989) 1012.

[9] R. D. S. G. Campilho, M. F. S. F. de Moura and J. J. M. S. Domingues, *Comp. Sci. Technol.* **65** (2005) 1948.

[10] R. D. S. G. Campilho, M. F. S. F. de Moura and J. J. M. S. Domingues, *Int. J. Sol. Struct.* **45** (2008) 1497